Lithographic characterization of the spherical error in an extreme-ultraviolet optic by use of a programmable pupil-fill illuminator

Patrick P. Naulleau, Jason P. Cain, and Kenneth A. Goldberg

Extreme-ultraviolet (EUV) lithography remains a leading contender for use in the mass production of nanoelectronics at the 32 nm node. Great progress has been made in all areas of EUV lithography, including the crucial issue of fabrication of diffraction-limited optics. To gain an accurate understanding of the projection optic wavefront error in a completed lithography tool requires lithography-based aberration measurements; however, making such measurements in EUV systems can be challenging. We describe the quantitative lithographic measurement of spherical aberration in a 0.3 numerical aperture. EUV microfield optic. The measurement method is based on use of the unique properties of a programmable coherence illuminator. The results show the optic to have 1 nm rms spherical error, whereas interferometric measurements performed during the alignment of the optic indicated a spherical error of less than 0.1 nm rms.

OCIS codes: 260.7200, 340.6720, 110.3960, 080.1010.

1. Introduction

Extreme-ultraviolet (EUV) lithography[1] is a leading candidate for use in high-volume manufacturing of nanoelectronic devices at feature sizes of 32 nm and below. Over the past several years, great progress has been made in all areas of EUV lithography, including the crucial issue of fabrication of diffraction-limited optics. Nevertheless, diffraction-limited high-numerical-aperture (NA) optics (larger than 0.2) remain a concern. The highest-NA EUV optics available to date are the 0.3 NA Micro-Exposure Tool (MET) optics used in an experimental exposure station at the Lawrence Berkeley National Laboratory (LBNL), Berkeley, California,[2,3] as well as commercial microfield EUV tools[4] used at at Intel and Sematech. Although interferometric measurements, both EUV and visible, have indicated diffraction-limited performance from these optics, lithographic verification of such performance has yet to be definitively demonstrated. This disconnect could arise from issues related to the alignment stability of the optic, conjugate point transfer from interferometry to imaging, accuracy of the interferometry, or combinations of these.

Accurate knowledge of the wavefront quality is essential for meaningful aerial-image modeling. To gain a better understanding of the optic wavefront error as installed in the lithography tool requires lithography-based quantitative aberration measurements. In this paper we present the quantitative lithographic measurement of spherical aberration of the 0.3-NA EUV optic in the LBNL MET tool. This 5×-reduction microfield optic comprises two aspherical optical elements and has a central obscuration with a radius equal to 30% of that of the full pupil.

The measurement method used to determine the spherical error is based on the use of the unique properties of a programmable coherence illuminator. The results show the optic to have a 1 nm rms spherical error, whereas interferometric measurements performed during the alignment of the optic nearly a year earlier indicated a spherical error of less than 0.1 nm rms.

2. Measurement Method

Various methods of print-based, quantitative aberration extraction have been proposed and imple-

P. P. Naulleau (pnaulleau@uamail.albany.edu) is with the College of Nanoscale Science and Engineering, University at Albany, New York 12203. J. P. Cain is with the Department of Electrical Engineering and Computer Science, University of California, Berkeley, California 94720. K. A. Goldberg is with the Center for X-Ray Optics, Lawrence Berkeley National Laboratory, Berkeley, California 94720.

Received 18 July 2005; accepted 21 October 2005.
0003-6935/06/091957-07$15.00/0

mented.[5–7] The problem with implementing these methods in the EUV, however, is that they typically rely on the use of phase-shift masks or on the ability to print at the diffraction limit of the optic. It is difficult to fabricate EUV pure phase-shift masks at any resolution, let alone at the diffraction-limited resolution required for aberration characterization. Moreover, current EUV resist technology is limited to resolving at approximately twice the diffraction limit of 0.3-NA EUV optics. These EUV-specific limitations preclude using the methods described in the literature for EUV applications at the present time.

Although ideally one would like to measure lithographically a wide range of optical aberrations (for example, the first 37 Zernike aberrations), quantitative measurement of even a few low-order aberrations would be extremely useful. For example, optical system alignment errors, such as those arising from drift, manifest themselves primarily as low-order aberrations such as astigmatism, coma, and spherical error. This is especially true for smaller-scale systems such as the MET optic, which comprises only two mirrors. Moreover, often the hardest aberrations to measure interferometrically are the low-order aberrations. As was demonstrated with the MET optic, one can readily quantify astigmatism in the EUV by measuring the orientation-dependent focus shift.[8] Here we concentrate on the quantitative measurement of spherical error by using a programmable coherence illuminator.

Spherical aberration can be viewed as a linear dependence of focus on radial offset in the pupil. The center of the optic, for example, focuses to a different longitudinal position than does the edge of the optic. Thus, when the diffraction pattern of the object being imaged, combined with the illumination pupil fill, occupies a significant radial range in the pupil, imaging performance will suffer. If this radially dependent focus shift can be measured lithographically, then the spherical error present in the optic can be quantified. In practice, when large pupil fills are used, such a measurement can be rather difficult owing to the inherent averaging of pupil characteristics over the area covered by the pupil fill. The use of small pupil fills, however, allows for isolation of small radial regions in the pupil. Furthermore, the ability to arbitrarily position the pupil fill provides for even more measurement flexibility. The programmable illuminator[9] available on the MET printing system at LBNL[2,3] is particularly well suited to these tasks.

One way to achieve the goal of sampling different radial locations in the pupil is to use diffraction from the object itself to set the radial sampling. Smaller-period line-space features will diffract the light farther in the pupil, allowing focus shift as a function of feature size to be used to characterize spherical error. The problem with this approach in a conventional unobscured optical system with a binary amplitude mask is that the zero diffraction order will be fixed to the center of the pupil as the diffracted orders move farther out. This in turn limits the sensitivity of the measurement because we cannot completely isolate the radial positions of interest.

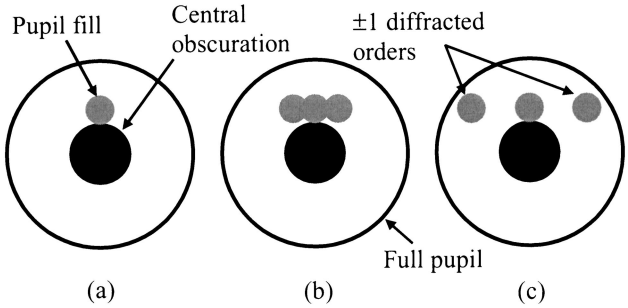

Fig. 1. Pupil-fill configuration enabling mask diffraction to be used to sample different radial offsets in the pupil while preventing the frequency-doubling problem from arising in the centrally obscured MET optic: (a) The pupil fill alone or in the presence of coarse lines and spaces on the mask, (b) the pupil fill modulated by the diffraction from a medium-pitch vertical line-space pattern on the mask, and (c) the pupil fill modulated by the diffraction from a fine-pitch vertical line-space pattern on the mask.

The radial isolation problem can be overcome by use of chromeless phase-shift mask architecture, which serves to suppress the zero-order term, leaving only the diffracted orders. Because the MET is an obscured system, however, mask-based zero-order suppression is not required; the pupil itself serves to eliminate the zero order when an appropriate pupil fill is used. Although zero-order elimination will effectively solve the potential sensitivity problem caused by ineffective radial isolation, the resultant printed pattern will be half as small as coded on the mask. This places stringent resolution requirements on the resist, which can be an issue in the EUV regime. For example, in a 0.3-NA EUV system, zero-order suppression corresponds to resolution requirements as small as 12 nm, well beyond current resist capabilities.

To overcome the resist resolution problem in the centrally obscured case, one can offset the pupil fill in the y direction to just clear the obscuration (Fig. 1). In this configuration, to prevent problems with obscuration of diffracted orders, only vertical lines and spaces (which diffract in the horizontal direction) should be used. This approach to solving the resolution problem, however, comes at the cost of incurring reduced sensitivity because of the isolation problem discussed above.

Another approach to sampling the pupil is to move the illumination in the pupil instead of relying on diffraction from the object (Fig. 2). In this case we can

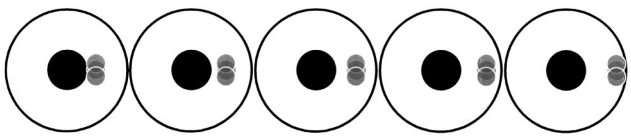

Fig. 2. Variable-offset-pupil-fill method for sampling radial positions in the optic. The pupil-fill pattern is shown modulated by a coarse horizontal line-space structure on the mask.

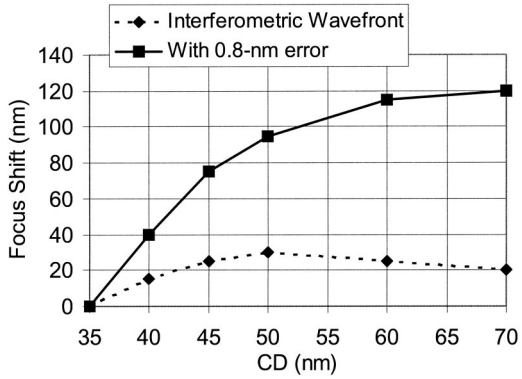

Fig. 3. Modeled focus as a function of feature half-pitch (CD) for the illumination configuration shown in Fig. 1. Two aberration conditions are considered in the model: The first is the wavefront error measured by EUV interferometry in late 2003, and the second is the same wavefront with the spherical error set to 0.8 nm rms. Note that the interferometrically measured wavefront includes approximately 0.1 nm rms spherical error.

use relatively coarse features and quantify the focus shift as a function of pupil fill position. To minimize edge effects from the pupil, the coarse features used to track focus are selected to diffract in a direction orthogonal to the pupil-fill offset. It is important to note that this technique relies on the use of a highly flexible pupil-fill illuminator such as the programmable scanning illuminator used in the LBNL EUV exposure station.[9]

3. Modeling

We modeled the two methods described above, using an aerial-image simulator, to test their effectiveness with the MET optic. The PROLITH software package[10] was used to compute the aerial image, and optimal contrast was used as the metric to determine best focus. In PROLITH modeling, two aberration conditions are considered; the first is the wavefront error that was measured by EUV interferometry in late 2003,[11] and the second is the same wavefront with the spherical error set to 0.8 nm rms. We note that the interferometrically measured wavefront includes approximately 0.1 nm rms spherical error as well as approximately 0.4 nm rms higher-order spherical error, among other aberrations. Figure 3 shows the resultant focus as a function of feature half-pitch, or critical dimension (CD). A total focus shift of ~120 nm is observed on going from 35 nm features to 70 nm features in the presence of 0.8 nm rms spherical error. In the expected wavefront condition, a focus shift of less than 30 nm is observed as the CD is increased. Despite incomplete radial isolation of the pupil sampling, this method provides sensitivity and selectivity adequate for characterization of spherical aberrations of the order of 0.3 nm rms or greater in the LBNL MET optic. It is important to note that this conclusion is valid only to the extent that the interferometric wavefront used[11] is still representative of the present aberrations in the LBNL MET.

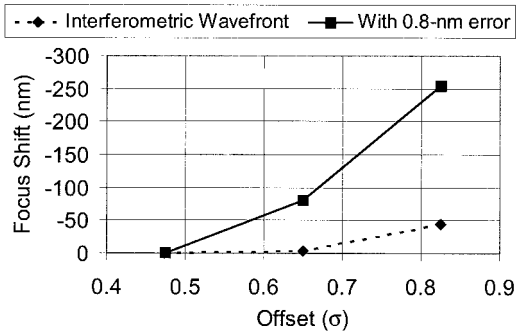

Fig. 4. Modeling results for the variable offset pupil-fill method. In this case, 0.8 nm spherical error causes a focus shift of greater than 250 nm as the pupil-fill offset σ is moved from 0.475 to 0.825. For the expected wavefront error the focus shift is less than 50 nm.

Figure 4 shows the modeling results for the variable-pupil-fill offset method. The focus shift was determined as the average value of 50, 60, and 70 nm equal line-space features. In this case, 0.8 nm spherical error causes a focus shift of greater than 250 nm as pupil-fill offset σ is moved from 0.475 to 0.825. For the expected wavefront error the focus shift is less than 50 nm. High sensitivity from this test is evident.

Although the modeling results show good sensitivity and selectivity for spherical error relative to the other aberrations that are present in the interferometrically measured wavefront, there remains the possibility that the interferometric measurement itself is not accurate or is no longer representative of the state of the optic. This concern is especially relevant for the low-order aberration components, which are most susceptible to mechanical alignment drifts in the optic and interferometric measurement error. To address this concern, the modeling is extended to further consider explicitly the measurement sensitivity to the astigmatism and coma Zernike terms. Figures 5 and 6 show the modeled focus shift, assuming that the wavefronts comprise isolated aberration terms: astigmatism (Z4 and Z5), coma (Z6 and Z7), and spherical error (Z8). In each case, 0.8 nm rms errors are considered.

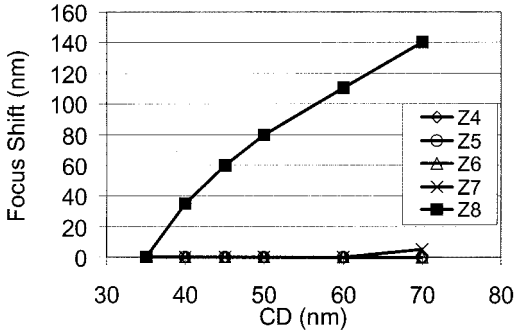

Fig. 5. Modeled sensitivity of the focus as a function of feature half-pitch (CD) to first-order aberrations. Astigmatism (Z4, Z5), coma (Z6, Z7), and spherical (Z8) aberrations are shown. Excellent selectivity to spherical error can be observed.

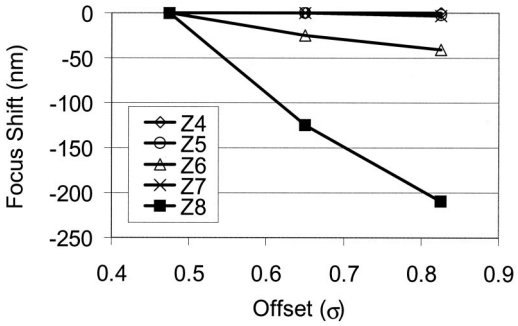

Fig. 6. Modeled sensitivity of the focus as a function of pupil-fill offset to first-order aberrations. Astigmatism (Z4, Z5), coma (Z6, Z7), and spherical (Z8) aberrations are shown. The only nonspherical term that shows any sensitivity is x-oriented coma. Because coma is an odd function, however, repeating the measurement on the opposite side of the pupil and averaging the results would serve as a means of eliminating sensitivity to coma. Of even more interest, these results indicate that pupil-dependent focus-shift methods can also potentially be used to quantify coma.

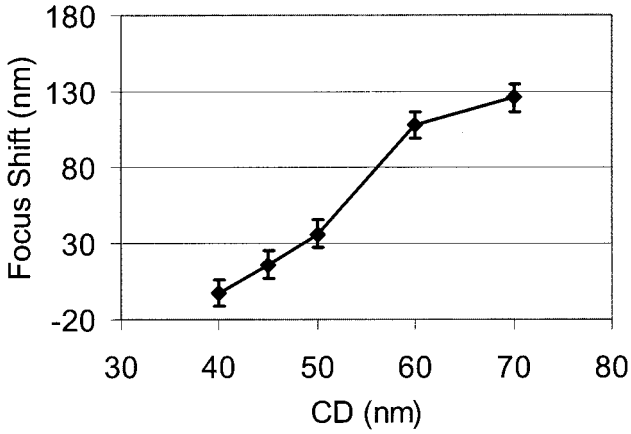

Fig. 7. Measured focus as a function of feature half-pitch (CD). The pupil fill was a disk of radius 0.15 σ positioned directly above the central obscuration in accordance with Fig. 1.

In the vast majority of cases, the methods show negligible sensitivity to nonspherical errors. The one exception is the sensitivity of the focus to pupil-fill offset in the presence of x-oriented coma. Because coma is an odd function, however, repeating the measurement on the opposite side of the pupil and averaging the results would serve as a means of eliminating sensitivity to coma. Of even more interest, these results indicate that pupil-dependent focus-shift methods can also potentially be used to quantify coma, although the relatively low sensitivity means that high accuracy is needed from the focus measurements in resist. This technique is currently being investigated for application to the MET optic.

It is important to note that, although good selectivity to other low-order aberrations has been shown, the method studied here does not provide selectivity to all the higher-order aberrations, for example, higher-order spherical errors. This is the reason for the signature observed in Figs. 3 and 4 for the interferometric wavefront; however, as evidenced by the same figures, the magnitude of higher-order aberrations in the MET is not large enough to significantly affect the sensitivity of the measurement to the primary spherical error of interest here. Of course, this statement is valid only to the extent that the interferometric data are accurate with respect to the higher-order terms and to the extent that these higher-order aberrations have remained constant. We note that published interferometry results[11] have shown these higher-order terms to be the most reproducible, lending credence to the above assumption.

4. Experimental Results

In this section we present results of experimental focus-shift measurement obtained from the MET optic at LBNL with the tests described above. In all cases the pupil fill was a disk of radius 0.15 σ. The resist used was a 125 nm thick layer of Rohm and Haas MET-1K.[12] The procedure for exposure of the CD-dependent focus-shift wafer is to generate a standard focus-exposure matrix. The best focus is then found for each feature size by analysis of the through-focus behavior of the printed feature size and line-edge roughness. In principle, the measurements could be further refined through full process-window analysis. To mitigate any concerns with respect to field curvature, the mask is designed such that the complete set of analyzed CDs falls within an area of approximately 10 μm × 10 μm out of the full 200 μm × 600 μm field size. For the pupil-fill-offset-dependent results, the exposure procedure is to generate a series of focus-exposure matrices on the same wafer, each one exposed by use of a different pupil-fill offset. The offset is chosen to lie in the x direction owing to the larger available pupil-fill range. The LBNL programmable illuminator supports a value of σ of as much as 1.2 in x and only 0.8 in y. A total of three offsets was used: $\sigma = 0.475, 0.65, 0.825$. To mitigate potential focus-control issues, we minimized the total exposed area by using only three dose values in each focus-exposure matrix. The total area covered by the multiple focus-exposure matrices on the single wafer is set to fall well within the leveled region of the wafer. Real-time focus control is provided by a glancing incidence laser-based print-site focus monitor that operates completely independently of the EUV beam.[13] Best focus from the prints is then found for one or more feature sizes for each pupil-fill offset. Focus was determined for horizontal features including half-pitches of 50, 60, and 70 nm features.

Figures 7 and 8 show plots of the measured focus as a function of CD and offset, respectively. We determine the error bars for the through-CD data by analyzing a separate focus-test wafer that comprises 10 through-focus columns, all at the same dose. The same metrology and focus-analysis methods as used for the spherical-test wafer are used to determine the best focus for each column of the focus-test wafer. Ignoring systematic column-to-column effects, the

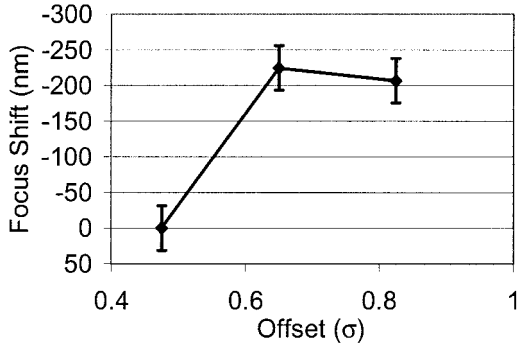

Fig. 8. Measured focus as a function of pupil-fill offset. The pupil fill was a disk of radius 0.15 σ and offset in the x direction. Three offsets were used: σ = 0.475, 0.65, 0.825.

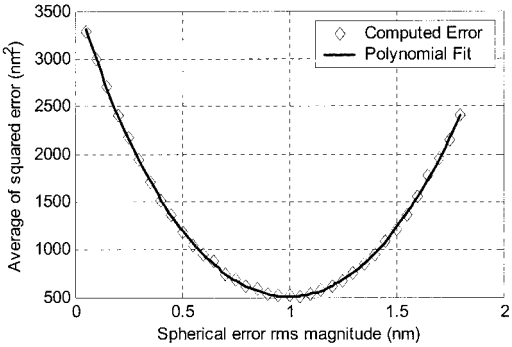

Fig. 10. Least-squares regression results to determine the expected value of the spherical aberration. The minimized function is the difference between the measured focus signature and the predicted focus signature as a function of the magnitude of spherical error. The predicted signature is determined through PROLITH modeling. Minimizing the error yields a predicted spherical aberration rms magnitude of 1 nm.

analysis of the focus-test wafer reveals an uncertainty in focus determination of approximately 9 nm.

For the offset-dependent focus shift we must be concerned further with focus errors that arise from location dependence within the array of the exposed die. This is so because we are now directly comparing the focus as measured in multiple columns in the in the array (each column corresponding to a different pupil offset setting), whereas, for the CD case, all the focus data are extracted from a single column in the exposed matrix. Thus exposure-position-dependent focus errors will be common to all CDs and need not be taken into consideration. To aid in the determination of the uncertainty and to ensure that the proper exposure dose was achieved, we included in the through-offset wafer three separate dose values for each offset, with each dose in its own column (Fig. 9). We found focus determination uncertainty by repeating the focus extraction at the three dose settings, which yielded an uncertainty of 31 nm.

5. Experimental Data Regression

It is evident from the results in Figs. 7 and 8 that the optic displays the signature of spherical aberration. To quantify this observation, a least-squares minimization approach is used. The function that we minimize is the difference between the measured focus signature and the predicted focus signature as a function of the magnitude of spherical error. The predicted signature is determined through PROLITH modeling, as used above for the representative case of 0.8 nm rms error.

Figure 10 shows the results of the minimization. The error function displays smooth behavior and a clear minimum. Minimizing the error, we find the predicted spherical aberration rms magnitude to be 1 nm. The rms of the residuals at the best fit is 48 nm. Given the focus measurement uncertainty described above and other potential error sources that arise when idealized aerial-image modeling is compared to printing in resist, the fit residual is consistent with expectation.

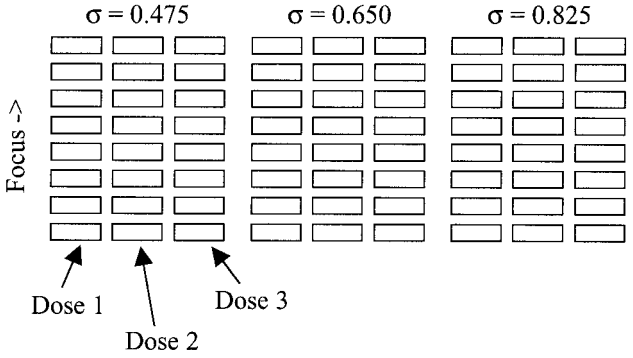

Fig. 9. Schematic of the exposure layout for the offset-dependent focus-shift wafer. Three separate focus-exposure matrices are exposed on the same wafer, with each matrix corresponding to a different pupil-fill offset. Because of wafer stage travel limits, only three dose values were used in each matrix.

6. Discussion

Printed image analysis from the MET optic at LBNL has revealed the presence of 1 nm rms spherical error. This is significantly higher than the value obtained during interferometric alignment of the optic. Potential causes of this discrepancy include field-point transfer error when one is switching from interferometry to imaging modes, alignment drift in the optic, and inaccuracies in the interferometric measurement. To gauge the relative likelihood of these errors, it is enlightening to consider the alignment sensitivity of the optic, including field-point alignment.

Table 1 shows the CODE V (Ref. 14) modeled annular Zernike rms magnitude sensitivities to misalignment states: M1 refers to the primary mirror; only the relative position changes between the primary and the secondary mirrors matter. The field point; corresponds to the object-plane position. Positive z moves are defined to be in the direction of propagation; thus a positive z move on M1 corresponds to increased separation between the two mirrors and a positive z move on the object plane corresponds to the plane moving closer to the optic. Zernike terms 0–3 (piston, tilt, and focus) are ignored. Moreover, Zernike terms above 8 are not

Table 1. Annular Zernike rms Magnitude Sensitivities to Misalignment States[a]

Zernike Number	M1					Field Point		
	+1 μm x	+1 μm y	+1 μm z	0.0001° x	0.0001° y	+1 mm x	+1 mm y	+1 mm z
4 (astig. 0°)	0.00	0.00	0.00	0.00	0.00	**0.09**	**−0.09**	0.00
5 (astig. 45°)	0.00	0.00	0.00	0.00	0.00	0.00	0.00	0.00
6 (coma x)	**0.53**	0.00	0.00	0.00	**0.08**	**−0.02**	0.00	0.00
7 (coma y)	0.00	**−0.53**	0.00	**0.08**	0.00	0.00	**0.02**	0.00
8 (spherical)	0.00	0.00	**0.05**	0.00	0.00	0.00	0.00	**2.49**

[a]M1 refers to the primary mirror; only the relative position changes between the primary and the secondary matter. The field point corresponds to the object-plane position. Positive z moves are defined to be in the direction of propagation; thus a positive z move on M1 corresponds to increased separation between the two mirrors and a positive z move on the object plane corresponds to the plane's moving closer to the optic. Zernike terms 0–3 (piston, tilt, and focus) are ignored. Moreover, Zernike terms above 8 are not shown because they all have negligible sensitivity to the alignment state of the optic. Bold face type signifies values greater than or equal to 0.005 nm.

shown because they all have negligible sensitivity to the alignment state of the optic. The only terms observed to affect spherical error are longitudinal separation of the two optics and longitudinal offset of the object plane. Table 1 shows that a 1 nm spherical error would correspond to a 20 μm longitudinal separation error between the two optics. We note that such a large alignment drift seems unlikely.

The other misalignment possibility would be a 400 μm longitudinal error in the placement of the object plane. Given that the system includes a reticle-plane metrology tower with three capacitive sensors to measure the height of the object plane[15] and that this metrology tower was also present during the interferometry, such a large placement error also seems unlikely. Moreover, the wafer-side height sensor was also present during the interferometry and served as a secondary field-point transfer metrology system. A 400 μm object-plane error corresponds to a 16 μm image-plane error. A change of this magnitude would actually be beyond the range of the sensor; thus it would not be possible for the object-plane metrology to be wrong without the image-sensor also having moved between interferometry and imaging. The only other remaining potential source for the discrepancy in spherical error would be an error in accuracy of the interferometry, which also seems unlikely.

In summary, pupil-position-dependent focus-shift measurements have been used to quantify the spherical aberration in a high-NA EUV optic. These measurements were made possible by the use of a programmable coherence illuminator. A 1 nm rms spherical error has been found in the MET, compared with the 0.1 nm value expected based on interferometry a year earlier. We have no definitive explanation for this change in spherical aberration; however, it is most likely due to interferometry errors or longitudinal placement error of the object plane. Although, in principle, errors are correctable through a 400 μm shift of the object plane, such a correction is not feasible in practice owing to range limits on the image-side wafer-height sensor. To correct this error, the height sensor would have to be repositioned, a complicated task that involves significant risk.

The authors are greatly indebted to Paul Denham and Brian Hoef of the Center for X-Ray Optics (CXRO) at Lawrence Berkeley National Laboratory for expert support with the exposure tool as well as to the entire CXRO engineering team for bringing the exposure tool to fruition. The authors thank Robert Brainard and Thomas Koehler of Rohm and Haas for resist and process support and Kim Dean of Sematech for programmatic support. This research was performed at Lawrence Berkeley National Laboratory and supported by Sematech. Lawrence Berkeley National Laboratory is operated under the auspices of the Director, Office of Science, Office of Basic Energy Science, of the U.S. Department of Energy.

References and Notes

1. R. Stulen and D. Sweeney, "Extreme ultraviolet lithography," IEEE J. Quantum Electron. **35,** 694–699 (1999).
2. P. Naulleau, K. Goldberg, J. Cain, E. Anderson, P. Denham, K. Jackson, S. Rekawa, F. Salmassi, and G. Zhang, "EUV microexposures at the ALS using the 0.3-NA MET optic," J. Vac. Sci. Technol. B **22,** 2962–2965 (2004).
3. P. Naulleau, K. Goldberg, E. Anderson, J. Cain, P. Denham, B. Hoef, K. Jackson, A. Morlens, S. Rekawa, and K. Dean, "EUV microexposures at the ALS using the 0.3-NA MET projection optics," in *Emerging Lithographic Technologies IX,* R. S. MacKay, ed., Proc. SPIE **5751,** 56–63 (2005).
4. A. Brunton, J. Cashmore, P. Elbourn, G. Elliner, M. Gower, P. Grunewald, M. Harman, S. Hough, N. McEntee, S. Mundair, D. Rees, P. Richards, V. Truffert, I. Wallhead, and M. Whitfield, "High-resolution EUV microstepper tool for resist testing and technology evaluation," in *High-Power Laser Ablation V,* C. R. Phipps, ed., Proc. SPIE **5448,** 681–692 (2004).
5. P. Dirksen, C. Juffermans, R. Pellens, M. Maenhoudt, and P. Debisschop, "Novel aberration monitor for optical lithography," in *Optical Microlithography XII,* L. Van den Hove, ed., Proc. SPIE **3679,** 77–86 (1999).
6. H. Fukuda, K. Hayano, and S. Shirai, "Determination of high-order lens aberration using phase/amplitude linear algebra," J. Vac. Sci. Technol. B **17,** 3318–3321 (1999).
7. G. Robins, K. Adam, and A. Neureuther, "Measuring optical image aberrations with pattern and probe based targets," J. Vac. Sci. Technol. B **20,** 338–343 (2002).
8. P. Naulleau, J. Cain, and K. Goldberg, "Lithographic characterization of the field dependent astigmatism and alignment

stability of a 0.3 numerical aperture EUV microfield optic," J. Vac. Sci. Technol. B (to be published).
9. P. Naulleau, K. Goldberg, P. Batson, J. Bokor, P. Denham, and S. Rekawa, "A Fourier-synthesis custom-coherence illuminator for EUV microfield lithography," Appl. Opt. **42,** 820–826 (2003).
10. PROLITH is a registered trademark of KLA-Tencor Corporation, 160 Rio Robles, San Jose, Calif. 95134.
11. K. Goldberg, P. Naulleau, P. Denham, S. Rekawa, K. Jackson, E. Anderson, and J. Liddle, "At-wavelength alignment and testing of the 0.3 NA MET optic," J. Vac. Sci. Technol. B **22,** 2956–2961 (2004).
12. R. Brainard, T. Koehler, P. Naulleau, and D. van Steenwinckel, "Performance of EUV photoresists on the ALS micro exposure tool," in *Emerging Lithographic Technologies IX,* R. S. Mackay, ed., Proc. SPIE **5751,** 754–764 (2005).
13. P. Naulleau, P. Denham, and S. Rekawa, "Design and implementation of a vacuum compatible laser-based subnanometer resolution absolute distance measurement system," Opt. Eng. **44,** 13,605–13,609 (2005).
14. CODE V is a registered trademark of Optical Research Associates, Suite 300, 3280 East Foothill Boulevard, Pasadena, Calif. 91107-3103.
15. P. Naulleau, K. Goldberg, E. Anderson, K. Bradley, R. Delano, P. Denham, B. Gunion, B. Harteneck, B. Hoef, H. Huang, K. Jackson, G. Jones, D. Kemp, A. Liddle, R. Oort, A. Rawlins, S. Rekawa, F. Salmassi, R. Tackaberry, C. Chung, L. Hale, D. Phillion, G. Sommargren, and J. Taylor, "Status of EUV microexposure capabilities at the ALS using the 0.3-NA MET optic," in *Emerging Lithographic Technologies VIII,* R. S. MacKay, ed., Proc. SPIE **5374,** 881–891 (2004).